Observing Single Molecules Complexing with Cucurbit[7]uril through Nanogap-SERS

Daniel O. Sigle,[†,¶] Setu Kasera,[‡,¶] Lars O. Herrmann,[†] Aniello Palma,[‡] Bart deNijs,[†] Felix Benz,[†] Sumeet Mahajan,[†] Jeremy J. Baumberg,[*,†] and Oren A. Scherman[*,‡]

†*Nanophotonics Centre, Cavendish Laboratory, University of Cambridge, Cambridge CB3 0HE, UK*

‡*Melville Laboratory for Polymer Synthesis, Department of Chemistry, University of Cambridge, Cambridge CB2 1EW, UK*

¶*Contributed equally to this work*

E-mail: jjb12@cam.ac.uk; oas23@cam.ac.uk

Abstract

In recent years, single molecule sensitivity achievable by surface-enhanced Raman spectroscopy (SERS) has been widely reported. We use this to investigate supramolecular host-guest chemistry with the macrocyclic host cucurbit[7]uril, on a few-to-single molecule level. A nanogap geometry, comprising individual gold nanoparticles on a planar gold surface spaced by a single layer of molecules, gives intense SERS. Plasmonic coupling between the particle and the surface leads to strongly enhanced optical fields in the gap between them, with single molecule sensitivity established using a modification of the well-known bi-analyte method. Changes in the Raman modes of the host molecule are observed when single guests included inside its cavity internally stretch it. Anisotropic intermolecular interactions with the guest are found which show additional distinct features in the Raman modes of the host molecule.

Graphical TOC Entry

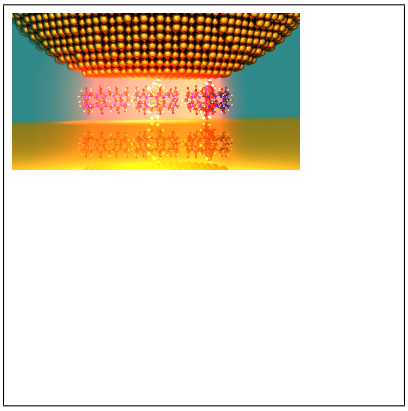

Keywords

single molecule sensitivity SERS, cucurbit[7]uril, host-guest chemistry, nanogaps, plasmons, bianalyte method, supramolecular chemistry, self-assembly

Single-molecule spectroscopy techniques have made remarkable contributions in understanding molecular chemistry, revealing details about molecule-surface interactions, molecular geometries and dynamic processes.[1,2] Surface-enhanced Raman spectroscopy (SERS) with its specific molecular fingerprinting capability, is a powerful analytical tool, requiring only simple experimental setups and sample handling. By placing molecules in strong plasmonic fields, the inherently weak Raman scattering cross-sections can be dramatically enhanced. This enables detecting substances at the single molecule level.[3–6] Until now, single molecule SERS has been primarily limited to detection and distinction between different chemical species. With the advent of analytical tools at single-molecule sensitivity,[2] characterization of intermolecular interactions have also drawn interest.[7–9] It is therefore important to extend the capabilities of SERS to investigate single-molecule chemical interactions.

A powerful plasmonic construct with a strong field confinement can be realized with the 'nanoparticle on mirror geometry' (NPoM),[10–12] where a gold nanoparticle (AuNP) is spaced above a flat Au surface by a single layer of molecules, establishing a plasmonic gap of only a few nanometres. Because the AuNP induces image charges within the metallic surface, plasmonic coupling similar to a nanoparticle dimer is created (Figure 1a,b). This self-assembled system thus creates a robust and reproducible plasmonic sensing platform for SERS with extremely high field localization, and is several orders of magnitude below the classical diffraction limit. Due to the strong confinement of the generated field enhancement, the interrogated volume only extends[13] over a few nm^3, and has shown promise in enabling down to single molecule resolution.[14,15]

We choose the macrocyclic host molecule cucurbit[7]uril (CB[7]) as a model system in this study. CB[7] belongs to a family of barrel-shaped molecular hosts, cucurbit[n]urils (CB[n]), which exhibit unique structural and chemical molecular recognition properties that make them suitable molecular receptors, particularly in aqueous systems.[16] The CB[7] host is able to bind a variety of 'guest' molecules such as cyclic and aromatic compounds, which are of interest for applications including environmental pollutant sensing,[17] materials design[18] and

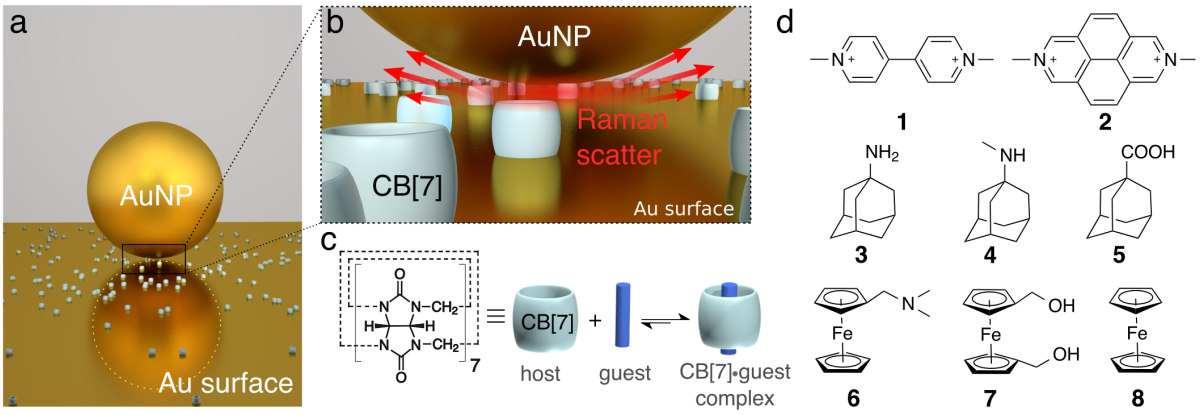

Figure 1: (a) Nanoparticle on mirror assembly. The AuNP is spaced from a gold surface by CB[7] molecules. (b) The plasmonically enhanced field in this construct is confined to a volume of only a few nm^3. (c) The macrocyclic host cucurbit[7]uril accommodates one guest molecule to form a host-guest complex. (d) Guest molecules investigated using the NPoM geometry: **1** methyl viologen, **2** 2,7 dimethyldiazapyrenium, **3** 1-adamantylamine, **4** N-methyl-1-adamantylamine , **5** 1-adamantane carboxylic acid, **6** (dimethylaminomethyl)ferrocene, **7** 1,1 ferrocene dimethanol and **8** ferrocene. Note: The counter-ion for the guests in all cases is chloride.

biomedical analyses.[19] Confined by the cavity volume of CB[7], only one guest molecule is typically encapsulated inside CB[7] at a given time (Figure 1c).

It is known from crystallographic studies that CB[n] undergoes structural deformations when its cavity is filled by a guest molecule.[20,21] Theoretical modelling with molecules such as **1** and **2** also predicts pronounced changes in the diameter of CB[7] when they are included inside its cavity as a guest.[22,23] These structural transformations are detected as shifts in the Raman vibrational frequencies of CB[n] as reported using a solution-based gold nanoparticle aggregate system.[24] It is also possible to study changes in the Raman signatures of guest molecules in bulk (solid) complexes.[25]

CB[7] is known to adsorb spontaneously on gold surfaces through interactions with the carbonyl portals, giving orientation of its barrel axis perpendicular to the gold surface.[26] Here, we use sparsely distributed gold nanoparticles on a planar gold surface separated by a fractional monolayer of complexed CB[7] molecules to fabricate a NPoM geometry with a fixed gap distance of $\sim$0.9 nm,[27] defined by the barrel height of the CB[7]. Guest molecules **1**-**8** (see Figure 1d), with reported binding affinities for CB[7] ranging from 10^5 to 10^{16} M^{-1} were investigated in this study[28] (see Supporting Information, section S2). Detailed examination

of the Raman modes of CB[7] and its complexes in the gap between particle and surface allows statistical analysis of the host-guest system.

Planar gold surfaces were prepared with a single physisorbed layer of CB[7] of fractional coverage (see Methods section). Colloidal AuNPs (diameter 100 nm) were then drop-cast on the surfaces in order to form NPoMs with strong field enhancements in the gaps. A distinction between the filled and unfilled states of the CB[7] cavities present within the NPoM plasmonic gaps can readily be observed using dark-field scattering microscopy. For example, the presence of MV^{2+} (**1**) within the CB[7] cavities shows clear red-shifts in the plasmonic resonances of the NPoM system (Figures 2a and 2b). The dominant plasmonic mode is a result of the coupling between the AuNP and the surface. These modes are observed at ∼730 nm when uncomplexed CB[7] is present in the NPoM gap whereas this mode shifts to ∼770 nm for gaps containing CB[7]·MV^{2+} instead. This is a result of the higher refractive index of the complexed CB[7].[29] The two cases were modelled using the boundary-element method (BEM) with refractive indices of the surrounding medium of $n = 1.2$ for the uncomplexed and $n = 1.5$ for the complexed state in order to qualitatively match the experimental data. The Raman excitation wavelength of 785 nm is thus close to the plasmonic gap resonances, allowing the vibrational spectral positions in the resulting SERS spectra to be compared.

CB[7] has many vibrational modes in the fingerprint region between 1100 cm^{-1} and 1500 cm^{-1} with two additionally pronounced peaks that stand out at lower frequencies (Fig.2c). The strongest mode at ∼440 cm^{-1} is a 'ring scissor mode', while the other strong mode, observed near 830 cm^{-1} is attributed to a 'ring breathing oscillation'.[30] When the macrocycle has a guest encapsulated inside its cavity, these CB[n] breathing modes undergo distortions[24,25] and provide a sensitive marker to distinguish between the filled and unfilled states of CB[7]. A typical SERS spectrum obtained from a single NPoM (Fig.2c) contains signatures from both CB[7] and MV^{2+}. The Raman bands observed using the NPoM are in agreement with those seen in solid reference samples for both the host and guest molecules

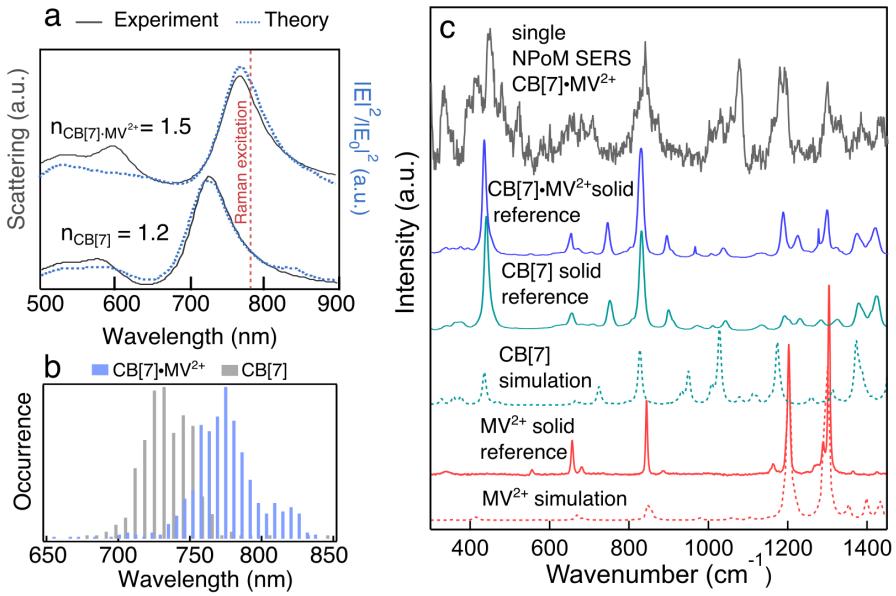

Figure 2: (a) Dark-field scattering spectra of NPoM with MV^{2+}·CB[7] and unfilled CB[7] as a spacer. The refractive index change caused by the guest leads to a shift of the plasmon resonance by 30 nm. Dotted (blue) lines are the corresponding field enhancements obtained by modelling for both cases. Vertical (red) dashed line indicates the Raman excitation wavelength ($\lambda = 785$ nm). (b) Statistical distribution of the dark-field scattering resonant wavelengths for unfilled CB[7] (grey) and MV^{2+}·CB[7] (blue) as spacers in the NPoM geometry. (c) From top to bottom: MV^{2+}·CB[7] SERS spectra on single NPoM, MV^{2+}·CB[7] complexed solid state Raman (experiment), CB[7] solid state Raman (experiment and simulation), MV^{2+} solid state (experiment and simulation).

as well as with simulations (using HF/3-21G, see Supporting Information, section S1).

Few molecule spectroscopy is highly sensitive to the immediate environment of the molecules being probed, which leads to inhomogeneous broadening and subtle fluctuations in the peak positions in individual spectra ($\pm 5\,\mathrm{cm}^{-1}$). Therefore, many individual spectra (on the order of 300 per molecule) as well as their averaged spectra are inspected. While Raman signals are often weak in individual spectra, they emerge as clearly visible bands in a stacked representation (Supporting Information, Figure S5).

On comparing the Raman spectra of solid CB[7] and that of CB[7] within the NPoM geometry, a new shoulder at $455\,\mathrm{cm}^{-1}$ becomes evident. This weak band is consistently observed across all the samples, including for the smaller homologue CB[5] and is likely to originate as a result of CB[n]-Au interactions (see section S3.2). Aside from this, shifts in the peak positions for the filled and unfilled states of CB[7] show differences depending on the guest molecule encapsulated inside the CB[7] cavity (Fig.3a). An extra signal at $\sim$445 cm^{-1} is also observed for **1**,**2**, **7** and **8**. This signal is, however, notably stronger for planar molecules **1** and **2**, which cause a pronounced ellipsoidal deformation of the CB[7] molecule. A different behavior is seen in cases with guests **3**-**8**, where the breathing mode at $440\,\mathrm{cm}^{-1}$ is shifted to a lower wavenumber at $\sim$435 cm^{-1}. The different shifts to higher or lower wavenumbers arise from the anisotropic interactions of the guest molecule with CB[7], depending on whether the guest molecules interact with only one or both of the two carbonyl portal rims (Figure 3b). A summary of the shifts in the peak position of CB[7] at $440\,\mathrm{cm}^{-1}$ for all the studied guests, and the fractional areas of the shifted signals, are shown in Figures 3(c,d). In general, the shifted mode is weaker (less area) than the unshifted CB[7] resonance. Guest molecules that interact with both portals exhibit shifts of the $440\,\mathrm{cm}^{-1}$ mode to high energy, while those that interact with only one portal shift to lower energy.

A similar trend is not observed for the mode at $830\,\mathrm{cm}^{-1}$ because this vibrational mode predominantly arises only from the equatorial region of the CB[7] and therefore, is relatively less affected by binding around the carbonyl portals. A slight shift towards lower frequency

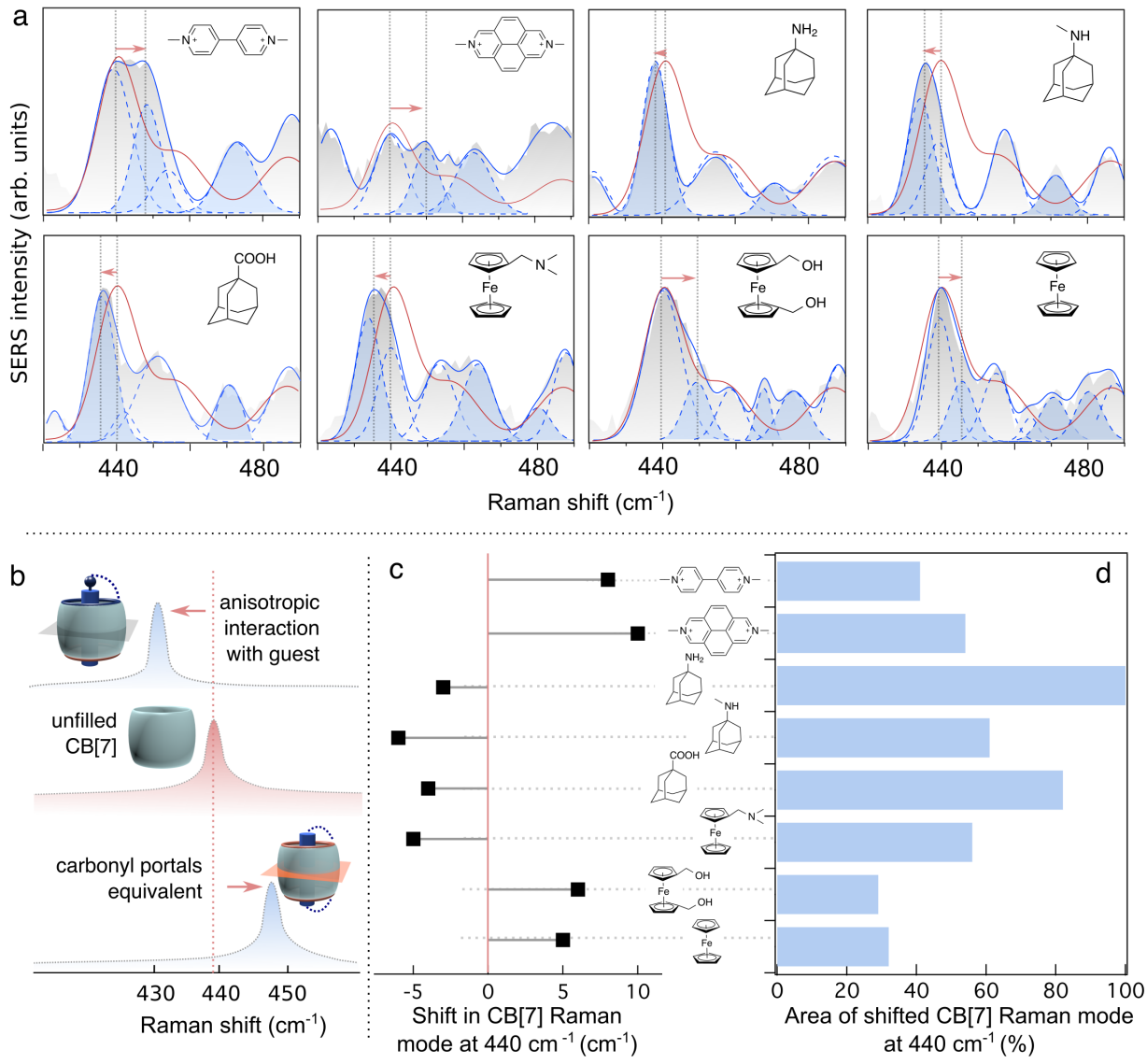

Figure 3: (a) Averaged SERS spectra of the CB[7] Raman modes near 440 cm^{-1} and showing the deconvolution (deconvoluted peaks shown with blue dashed lines), with peaks attributed to filled CB[7] colored blue. The fitted spectra for CB[7] control in the absence of guest has been overlayed (red) in each case for comparison. (b) Schematic showing characteristic trends in shifts. (c) Size of shifts and (d) areas of the shifted CB[7] vibrational mode at 440 cm^{-1} for each guest molecule (%, relative to unfilled CB[7]).

($\sim$827 cm^{-1}) is observed in all cases, while an additional broad signal can be observed at $\sim$870 cm^{-1} including control samples (of CB[7] and CB[5]). These signals are therefore, again likely to arise from the electrostatic interaction of CB[n] with the gold surface. While similar magnitudes for such shifts have been shown in SERS using colloidal gold nanoparticle aggregates,[24] the different effects of different molecules have not been reported before.

When probing the distribution of the complexed and uncomplexed states of CB[7] in individual NPoMs with only a few molecules in each plasmonic nanojunction, three different situations can be observed (Figure 4a): (i) the probed CB[7] molecules are unfilled, resulting in *unshifted* CB[7] Raman modes; (ii) both filled and unfilled states of CB[7] or 'mixed events' are detected simultaneously in cases where more than one molecule may be present in the gap; and (iii) all CB[7] molecules in the junction each contain a guest, leading to only the *shifted* Raman modes. Representative spectra showing the 400 cm^{-1} and 800 cm^{-1} regions for **1** are shown in Figure 4b (see Supporting Information, Figures S8-S10 for individual spectra of other guest molecules).

For all the guest CB[7] inclusion complexes, 40%-60% of the investigated NPoMs exhibit either only filled or only unfilled CBs, which strongly suggests that the SERS signal is in many instances generated by single molecules (Figure 4). The mixed events, however, may arise in three cases: (1) more than one molecule is probed, (2) CB[7] host-guest complexes, in general, are known to be dynamic due to the 'in-and-out' diffusion of guests from the CB[7] cavity. These diffusional movements are much faster compared to the integration time (10 seconds) used for measurement of SERS spectra. For example, the lifetime of MV^{2+}·CB[7] is reported to be 5.3$\pm$0.5 miliseconds.[31] Therefore, it is possible that in some cases, depending on the local environment of the complexed molecule, a *temporal averaging effect* is observed due to this diffusion. In these cases, signals may be obtained from the same CB[7] molecule in a filled and unfilled state. (3) Similarly, it is also possible that the incident laser occasionally removes the guest molecules from the CB[7] cavity, also resulting in a temporal average signal being observed. In cases (2) and (3), the mixed event signals could arguably also be

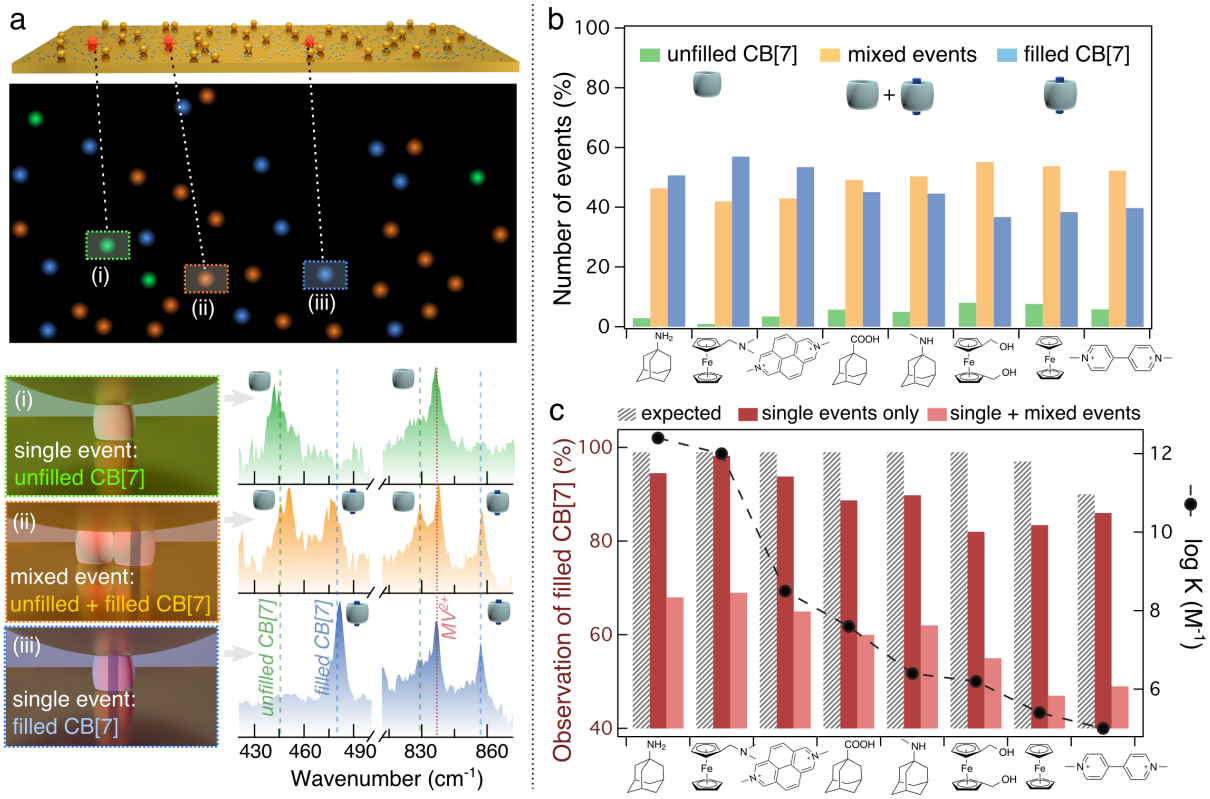

Figure 4: (a) (top) Schematic illustration of distribution of the underlying composition of the CB[7] and MV^{2+}·CB[7] mixture in the NPoM probes showing three observable events. (bottom) Individual SERS spectra of the two predominant CB[7] Raman modes near 440 cm^{-1} and 830 cm^{-1} (CB[7] modes are highlighted with grey dashed lines and MV^{2+} modes with red dotted lines). Spectra correspond to (i) NPoM with purely unfilled CB[7] (green), (ii) a mix of filled and unfilled CB[7] (orange), and (iii) only filled CB[7] (blue). (b) Statistical representation of the number of events observed. For each guest molecule, the statistics is based on the investigation of between 300–400 NPoMs with sufficiently strong SERS signals to enable identification of the relevant modes. (c) Comparison of the number of times signals from filled CB[7] is observed for single molecule events only and mixed events as a function of decreasing order of binding affinities of guests for CB[7]. Overlayed trace shows log of binding strengths of the guest molecules for CB[7].

attributed to single molecules.

The high number of single molecule events suggests somehow additional field localization addresses only a few molecules. Possibly this arises from imperfections and adatoms raised above the plain surface in the nanogap architecture that can localize light to even smaller volumes than the gap plasmon, and thus play a significant role in promoting selected molecules to produce more intense SERS by creating strong locally concentrated electric fields.[32]

The method presented here is thus built upon the well-established bi-analyte technique, which is used to demonstrate single molecule sensitivity.[33–35] Typically the SERS of a mixture of two different chemical species is investigated where the occurrence of only one of the two species in a spectrum is an indication that it originates from only one molecule. In the study here, the SERS signals from only the host molecule are monitored, with the *filled* and *unfilled* states of CB[7] (with a guest) now treated as two distinct species. The signatures of the two states are compared *via* the energy shift of Raman bands upon complexation. In addition to its simplicity, one of the main advantage of this method is that it enables every active site to be probed and to determine single-molecule sensitivity without relying on accurate determination of the number of molecules in the nanogap.

Based on the known 1:1 binding stoichiometry and association constants of the guests towards CB[7][36–39] (see Table S1), the fraction of CB[7] that should be in a complexed state can be estimated using the Hill equation.[40] For the concentration used in these experiments, the fraction of CB[7] expected to be in a filled state ranges from ∼90% for the weaker binding guests such as **1** and **2** to ∼99% for the strong binders (**3**–**5**). These theoretical fractions were compared with the number of experimental observations of Raman signals from filled CB[7] in approximately 350 spectra (i.e. number of spectra containing shifted CB[7] signals). In general, guests that bind to CB[7] with a strong affinity showed a higher frequency of observations from filled CB[7]. This phenomenon is also evident in the averaged spectra, where these molecules show a weaker band from unfilled CB[7] (Figure 3). Furthermore, a control study using 1:10 MV^{2+}·CB[7] (10 μM MV^{2+}:100 μM CB[7]) in the NPoM geometry

showed a significant increase in the number spectra containing empty CB[7] single events compared to the number of filled CB[7] events (Supporting Information, Figure S7). The number of mixed events observed was also lower. These results indicate that the populations of filled and unfilled CB[7] on the gold surfaces are likely not a random distribution of the two states but rather are determined by the binding affinity of the guest towards CB[7]. This is not surprising: the formation of a complex between a host and a guest molecule is a fundamental process in supramolecular chemistry and a variety of interactions and energies are collectively involved.[40,41] Therefore, the molecules would be expected to reside inside the CB[7] cavity governed by their respective association constants. This observation is consistent with a study investigating the recognition properties of self-assembled monolayers of CB[7] with atomic force microscopy.[42]

From within the hundreds of spectra analysed for each guest, only spectra showing either *only filled* CB[7] or *only unfilled* CB[7] (i.e. single events) were selected. $> 80\%$ of these single event spectra were found to originate from *only filled CB[7]* (Figure 4c), which is close to the aforementioned expected range of 90-99%. However, if the *single event only* spectra was not pre-selected and all the collected spectra including mixed events were taken into account, the fraction of filled CB[7] was found to be lower i.e. 45-60%. (Figure 4c). In our analyses, a mixed event is assumed to originate from one filled CB[7] molecule and one unfilled CB[7] molecule, whereas the actual number of molecules contributing to the signals in mixed events is unknown. Therefore, the discrepancies in the expected and observed number of filled CB[7] events can be reasonably well accounted for. The probable removal of guest from the CB[7] cavity by the laser light (as suggested earlier) might also lead to a lower fraction of filled CB[7] than expected.

The intensities of the SERS signals obtained from different NPoMs vary by roughly a factor of 10, despite the well defined orientation of both molecules and optical fields. A major contributing factor to these variations in SERS intensities is the total number of molecules present in the enhanced field region in the gap, which depends on the precise

volume of the cavity formed by the AuNP and substrate, set by the facetting of the NP. The 100 nm diameter AuNPs used in these experiments exhibit typical facet diameters between ∼5 nm and 50 nm, resulting in up to hundred-fold variations of the number of incorporated molecules (see Supporting Information, section S6). Assuming a tightly packed monolayer of CB[7], a small AuNP facet with a 5 nm diameter can accommodate approximately 40 CB[7] molecules inside the nanogap, while a large facet of 50 nm can hold up to 4000 molecules. In this case, however, using dilute solutions of CB[7] to form sparse monolayers, it is estimated that there are typically between 1-100 CB[7] molecules in each NPoM gap.

While perfectly spherical AuNPs would lead to similar detection volumes in each NPoM, the actual cavity size varies as a consequence of the pronounced AuNP facetting. Driven by van der Waals interactions, faceted nanoparticles predominantly tend to align their facets parallel to the underlying substrate[43] (Supporting Information, Figure S11). This forms a nanoscopic plasmonic cavity,[44] which supports standing waves with nodes of high and low field enhancements and of sizes defined by the width of the facet. The specific location of the molecules within the gap as well as the in- and out-coupling efficiency of light, therefore becomes an important factor in determining the scattering intensity.

Furthermore, the field enhancement and field distribution within the nanogap is highly sensitive to the exact morphology of the NPoM construct.[45] Inherent nanometre-scale defects exist on the surface of the AuNP as well as on the underlying gold mirror. This creates extremely strong and highly localized fields in particular areas within the gap through an additional lightning-rod effect.[46] Molecules in the vicinity of these 'sub-hot spots' potentially produce a much higher SERS intensity. Additional intensity variations are also partly caused by alignment mismatches between the laser and the symmetry axis of the NPoM resulting in fluctuations of the field enhancement.

In conclusion, we show that SERS spectroscopy of individual NPoMs can clearly distinguish between the different kinetic states (filled or unfilled) of the CB[7] molecules within the NPoM plasmonic nanogap. While it is common to use resonant dye molecules with

strong Raman responses to demonstrate single molecule resonant SERS (SERRS),[47] the results presented here confirm that few-to-single molecule sensitivity can also be achieved with electronically *non-resonant* molecules.[48] However, single molecule resolution is not comprehensively achieved in all NPoMs and it is anticipated that the actual number of traced molecules depends on the exact morphology of the AuNP and the Au surface.

We observe subtle differences in SERS peak positions and their respective broadening or fluctuations depending on the guest bound into the CB[7]. It is also clear that any substituents covalently interacting with only one of the carbonyl portals of CB[7] exerts a considerable influence on its structure. We evidence clear effects from the symmetry of the guest molecules, which should now guide the development of more accurate theoretical models of the host-guest binding configuration. Furthermore, the applicability of this system in direct statistical estimation of the number of filled CB[7] on a surface is demonstrated and may be extended to interrogate host-guest systems in a similar manner. This concept opens up opportunities to establish host-guest chemistry as a single molecule sensing platform useful for gas sensing, drug detection[49] or quantitative sensing of various hazardous substances. Further, it could be used to investigate guest binding properties for a variety of biologically significant molecules such as peptides, DNA, lipid membranes, and allows real-time observation of chemical reaction kinetics.

Experimental

Flat gold surfaces were prepared using electron-beam evaporation. A 5 nm thick chromium adhesion layer was deposited on a silicon wafer, followed by a 70 nm thick gold film. Host-guest complex solutions were prepared by mixing guest molecules and CB[7] (100 μM, 1:1 stoichiometry) followed by sonication for approximately 5 minutes. Less water-soluble guest molecules (such as ferrocene) required longer sonication times ($\sim$30 minutes). Gold surfaces were functionalized by immersion in the host-guest solution for at least 24 h to allow formation of a distorted and sparsely distributed CB[7] monolayer on the surface. Samples were then rinsed with water and blow-dried. 100 nm citrate-capped colloidal AuNPs (BBI solutions) were drop cast on the sample surface where

physisorption takes place. After 5 min, excess NPs were washed away.

Raman microscopy was performed on a Renishaw inVia Raman microscope using a 100x objective with numerical aperture, NA=0.85. To match the plasmon resonance, an excitation wavelength of 785 nm was chosen with optical power in the objective set to 13 mW. Integration time was 10 s. The SERS spectra were collected on single mirror-coupled AuNPs. This was done by identifying individual AuNPs using dedicated bright- and darkfield-imaging in order to move them to the center of the objective to which the Raman laser was aligned as well.
SERS signals could not be observed when the Raman laser was not centered on a nanoparticle i.e. nothing but background noise was observed. Further, there were cases when SERS signals were not obtained even with 'on-particle' measurements. This is expected to happen if the nanoparticle being studied is not located on adsorbed molecules as they are only sparsely distributed on the surface. Samples for reference Raman spectra of MV^{2+}·CB[7] was obtained by freeze-drying a 1 mM (1:1) solution of the complex.

Optical scattering spectra were taken on an Olympus BX51 research microscope in dark-field configuration using a 100x objective with numerical aperture NA=0.85. The samples were illuminated using a halogen white light source and scattered light was collected with a multimode fibre in confocal configuration attached to a cooled spectrometer.

The near-field enhancement inside the nanogap was modelled with the boundary element method using BEMAX.[50,51] The CB[7] and MV^{2+}·CB[7] molecular spacers were modelled as a layer of constant refractive index with $n = 1.2$ and $n = 1.5$, respectively,[29] between a flat Au surface and an AuNP. The dielectric functions of Au were taken from Johnson and Christy.[52] The illumination source was a broadband plane-wave, incident at an angle of 58° to account for NA=0.85 in the experimental setup.

Acknowledgement

The authors acknowledge funding from Walters-Kundert Trust, EPSRC (EP/K028510/1, EP/G060649/1, EP/ H007024/1, ERC LINASS 320503), an ERC starting investigator grant (ASPiRe 240629), EU CUBiHOLE grant and the Defence Science and Technology Laboratory (DSTL). S.K. thanks Krebs

Memorial Scholarship (The Biochemical Society) and Cambridge Commonwealth Trust for funding.

Supporting Information Available

ITC characterization of CB[7] binding with guest molecules **4** and **7**, control studies, additional representations of the SERS spectra, SEM characterization of sample and estimation of number of molecules in NPoM gaps. This material is available free of charge via the Internet at `http://pubs.acs.org/`.

References

(1) Tamarat, P.; Maali, A.; Lounis, B.; Orrit, M. Ten Years of Single-Molecule Spectroscopy. *J. Phys. Chem. A* **2000**, *104*, 1–16.

(2) Claridge, S. A.; Schwartz, J. J.; Weiss, P. S. Electrons, Photons, and Force: Quantitative Single-Molecule Measurements from Physics to Biology. *ACS Nano* **2011**, *5*, 693–729.

(3) Kneipp, K.; Wang, Y.; Kneipp, H.; Perelman, L.; Itzkan, I.; Dasari, R.; Feld, M. Single Molecule Detection Using Surface-Enhanced Raman Scattering (SERS). *Phys. Rev. Lett.* **1997**, *78*, 1667–1670.

(4) Nie, S.; Emory, S. R. Probing Single Molecules and Single Nanoparticles by Surface-Enhanced Raman Scattering. *Science* **1997**, *275*, 1102–1106.

(5) Cialla, D.; März, A.; Böhme, R.; Theil, F.; Weber, K.; Schmitt, M.; Popp, J. Surface-Enhanced Raman Spectroscopy (SERS): Progress and Trends. *Anal. Bioanal. Chem.* **2012**, 27–54.

(6) Lee, H. M.; Jin, S. M.; Kim, H. M.; Suh, Y. D. Single-Molecule Surface-Enhanced Raman Spectroscopy: A Perspective on the Current Status. *Phys. Chem. Chem. Phys.* **2013**, *15*, 5276–5287.

(7) Eckel, R.; Ros, R.; Decker, B.; Mattay, J.; Anselmetti, D. Supramolecular Chemistry at The Single-Molecule Level. *Angew. Chem. Int. Ed.* **2005**, *44*, 484–8.

(8) Yasuda, S.; Okutsu, Y.; Suzuki, I.; Shinohara, K.-I.; Komiyama, M.; Takeuchi, O.; Shigekawa, H. Single Molecular Anatomy of Host-Guest Chemistry Based on Atomic Force Microscopy Study of Cyclodextrin-Ferrocene Molecular Interaction. *Jpn. J. Appl. Phys.* **2007**, *46*, 5614–5616.

(9) Beulen, M. W. J.; Huskens, J.; Veggel, F. C. J. M. V.; Reinhoudt, D. N.; Vancso, G. J. Individual Supramolecular Host - Guest Interactions Studied by Dynamic Single Molecule Force Spectroscopy. *J. Am. Chem. Soc.* **2000**, 4963–4967.

(10) Aravind, P.; Rendell, R.; Metiu, H. A New Geometry for Field Enhancement in Surface-Enhanced Spectroscopy. *Chem. Phys. Lett.* **1982**, *85*, 396–403.

(11) Mock, J. J.; Hill, R. T.; Degiron, A.; Zauscher, S.; Chilkoti, A.; Smith, D. R. Distance-Dependent Plasmon Resonant Coupling between a Gold Nanoparticle and Gold Film. *Nano Lett.* **2008**, *8*, 2245–2252.

(12) Ciraci, C.; Hill, R. T.; Mock, J. J.; Urzhumov, Y.; Fernandez-Dominguez, A. I.; Maier, S. A.; Pendry, J. B.; Chilkoti, A.; Smith, D. R. Probing the Ultimate Limits of Plasmonic Enhancement. *Science* **2012**, *337*, 1072–1074.

(13) Sigle, D. O.; Hugall, J. T.; Ithurria, S.; Dubertret, B.; Baumberg, J. J. Probing Confined Phonon Modes in Individual CdSe Nanoplatelets Using Surface-Enhanced Raman Scattering. *Phys. Rev. Lett.* **2014**, *113*, 1–5.

(14) Li, L.; Hutter, T.; Steiner, U.; Mahajan, S. Single Molecule SERS and Detection of Biomolecules with a Single Gold Nanoparticle on a Mirror Junction. *Analyst* **2013**, *138*, 4574–8.

(15) Taylor, R. W.; Benz, F.; Sigle, D. O.; Bowman, R. W.; Bao, P.; Roth, J. S.; Heath, G. R.; Evans, S. D.; Baumberg, J. J. Watching Individual Molecules Flex Within Lipid Membranes Using SERS. *Sci. Rep.* **2014**, *4*, 1–6.

(16) Masson, E.; Ling, X.; Joseph, R.; Kyeremeh-Mensah, L.; Lu, X. Cucurbituril Chemistry: A Tale of Supramolecular Success. *RSC Adv.* **2012**, *2*, 1213–1247.

(17) Yao, F.; Liu, H.; Wang, G.; Du, L.; Yin, X.; Fu, Y. Determination of Paraquat in Water Samples Using a Sensitive Fluorescent Probe Titration Method. *J. Environ. Sci.* **2013**, *25*, 1245–1251.

(18) Ahn, Y.; Jang, Y.; Selvapalam, N.; Yun, G.; Kim, K. Supramolecular Velcro for Reversible Underwater Adhesion. *Angew. Chem. Int. Ed.* **2013**, *52*, 3140–3144.

(19) Kasera, S.; Herrmann, L. O.; del Barrio, J.; Baumberg, J. J.; Scherman, O. A. Quantitative Multiplexing with Nano-Self-Assemblies in SERS. *Sci. Rep.* **2014**, *4*, 6785.

(20) Freeman, B. Y. W. A.; Freeman, W. A. Structures of the P-Xylylenediammonium Chloride and Calcium Hydrogensulfate Adducts of the Cavitand Cucurbituril. *Acta Cryst.* **1984**, *b40*, 382–387.

(21) Huang, W.-H. H.; Zavalij, P. Y.; Isaacs, L. Cucurbit[6]uril P-Xylylenediammonium Diiodide Deca-Hydrate Inclusion Complex. *Acta Cryst.* **2008**, *64*, o1321–o1322.

(22) El-Barghouthi, M. I.; Assaf, K. I.; Rawashdeh, A. M. M. Molecular Dynamics of Methyl Viologen-Cucurbit[n]uril. *J. Chem. Theory Comput.* **2010**, *6*, 984–992.

(23) Sindelar, V.; Cejas, M. A.; Raymo, F. M.; Kaifer, A. E. Tight Inclusion Complexation of 2,7-Dimethyldiazapyrenium in Cucurbit[7]uril. *New J. Chem.* **2005**, *29*, 280–282.

(24) Kasera, S.; Biedermann, F.; Baumberg, J. J.; Scherman, O. A.; Mahajan, S. Quantitative SERS Using the Sequestration of Small Molecules Inside Precise Plasmonic Nanoconstructs. *Nano Lett.* **2012**, *12*, 5924–5928.

(25) Chen, Y.; Klimczak, A.; Galoppini, E.; Lockard, J. V. Structural Interrogation of a Cucurbit[7]uril-Ferrocene HostGuest Complex in the Solid State: A Raman Spectroscopy Study. *RSC Adv.* **2013**, *3*, 1354–1358.

(26) An, Q.; Li, G.; Tao, C.; Li, Y.; Wu, Y.; Zhang, W. A General and Efficient Method to Form Self-assembled Cucurbit[n]uril Monolayers on Gold Surfaces. *Chem. Comm.* **2008**, 1989–1991.

(27) Taylor, R. W.; Lee, T.-C.; Scherman, O. A.; Esteban, R.; Aizpurua, J.; Huang, F. M.; Baumberg, J. J.; Mahajan, S. Precise Subnanometer Plasmonic Junctions for SERS within Gold Nanoparticle Assemblies Using Cucurbit[n]uril "Glue". *ACS Nano* **2011**, *5*, 3878–3887.

(28) Barrow, S. J.; Kasera, S.; Rowland, M. J.; del Barrio, J.; Scherman, O. A. Cucurbituril-Based Molecular Recognition. *Chem. Rev.* **2015**, *115*, 12320–12406.

(29) deNijs, B.; Bowman, R. W.; Herrmann, L. O.; Benz, F.; Barrow, S. J.; Mertens, J.; Sigle, D. O.; Chikkaraddy, R.; Eiden, A.; Ferrari, A. et al. Unfolding the Contents of Sub-nm Plasmonic Gaps Using Normalising Plasmon Resonance Spectroscopy. *Farad. Discuss.* **2015**, *178*, 185–193.

(30) Mahajan, S.; Lee, T.-C.; Biedermann, F.; Hugall, J. T.; Baumberg, J. J.; Scherman, O. A. Raman and SERS Spectroscopy of Cucurbit[n]urils. *Phys. Chem. Chem. Phys.* **2010**, *12*, 10429–10433.

(31) Kim, H.-J.; Jeon, W. S.; Ko, Y. H.; Kim, K. Inclusion of Methylviologen in Cucurbit[7]uril. *Proc. Natl. Acad. Sci.* **2002**, *99*, 5007–5011.

(32) Otto, A.; Billmann, J.; Eickmans, J.; Erturk, U.; Pettenkofer, C. The Adatom Model of SERS (Surface Enhanced Raman-Scattering) - The Present Status. *Surface Science* **1984**, *138*, 319–338.

(33) Etchegoin, P. G.; Le Ru, E. C.; Fainstein, A. Bi-analyte Single Molecule SERS Technique with Simultaneous Spatial Resolution. *Phys. Chem. Chem. Phys.* **2011**, *13*, 4500–4506.

(34) Le Ru, E. C.; Meyer, M.; Etchegoin, P. G. Proof of Single-Molecule Sensitivity in Surface Enhanced Raman Scattering (SERS) by Means of a Two-Analyte Technique. *J. Phys. Chem. B* **2006**, *110*, 1944–1948.

(35) Patra, P. P.; Kumar, G. V. P. Single-Molecule Surface-Enhanced Raman Scattering Sensitivity of Ag-Core Au-Shell Nanoparticles: Revealed by Bi-Analyte Method. *J. Phys. Chem. Lett.* **2013**, *4*, 1167–1171.

(36) Ong, W.; Kaifer, A. E. Unusual Electrochemical Properties of the Inclusion Complexes of Ferrocenium and Cobaltocenium with Cucurbit[7]uril. *Organometallics* **2003**, *22*, 4181–4183.

(37) Ong, W.; Kaifer, A. E. Salt Effects on the Apparent Stability of the Cucurbit[7]uril–Methyl Viologen Inclusion Complex. *J. Org. Chem* **2004**, *69*, 1383–1385.

(38) Liu, S.; Ruspic, C.; Mukhopadhyay, P.; Chakrabarti, S.; Zavalij, P. Y.; Isaacs, L. The Cucurbit[n]uril Family: Prime Components for Self-Sorting Systems. *J. Am. Chem. Soc.* **2005**, *127*, 15959–15967.

(39) Jeon, W. S.; Moon, K.; Park, S. H.; Chun, H.; Ko, Y. H.; Lee, J. Y.; Lee, E. S.; Samal, S.; Selvapalam, N.; Rekharsky, M. V. et al. Complexation of Ferrocene Derivatives by the Cucurbit[7]uril Host: A Comparative Study of the Cucurbituril and Cyclodextrin Host Families. *J. Am. Chem. Soc.* **2005**, *127*, 12984–12989.

(40) Schalley, C. In *Analytical Methods in Supramolecular Chemistry*; Schalley, C., Ed.; Wiley-VCH Verlag GmbH & Co. KGaA: Weinheim, Germany, 2006.

(41) Izatt, R. M.; Bradshaw, J. S.; Pawlak, K.; Bruening, R. L.; Tarbet, B. J. Thermodynamic and Kinetic Data for Macrocycle Interaction with Neutral Molecules. *Chem. Rev.* **1992**, *92*, 1261–1354.

(42) Gomez-Casado, A.; Jonkheijm, P.; Huskens, J. Recognition Properties of Cucurbit[7]uril Self-Assembled Monolayers Studied with Force Spectroscopy. *Langmuir* **2011**, *27*, 11508–11513.

(43) Harfenist, S. A.; Wang, Z. L.; Alvarez, M. M.; Vezmar, I.; Whetten, R. L. Highly Oriented Molecular Ag Nanocrystal Arrays. *J. Phys. Chem.* **1996**, *100*, 13904–13910.

(44) Sigle, D. O.; Mertens, J.; Herrmann, L. O.; Bowman, R. W.; Ithurria, S.; Dubertret, B.; Shi, Y.; Yang, H. Y.; Tserkezis, C.; Aizpurua, J. et al. Monitoring Morphological Changes in 2D Monolayer Semiconductors Using Atom-Thick Plasmonic Nanocavities. *ACS Nano* **2014**, *9*, 825–830.

(45) Doering, W. E.; Nie, S. Single-Molecule and Single-Nanoparticle SERS : Examining the Roles of Surface Active Sites and Chemical Enhancement. *J. Phys. Chem. B* **2002**, *106*, 311–317.

(46) Liao, P. F.; Wokaun, A. Lightning Rod Effect in Surface Enhanced Raman Scattering. *J. Chem. Phys.* **1982**, *76*, 751–752.

(47) Patra, P. P.; Chikkaraddy, R.; Tripathi, R. P. N.; Dasgupta, A.; Kumar, G. V. P. Plasmofluidic Single-Molecule Surface-Enhanced Raman Scattering from Dynamic Assembly of Plasmonic Nanoparticles. *Nat. Commun.* **2014**, *5*, 4357.

(48) Blackie, E. J.; Ru, E. C. L.; Etchegoin, P. G. Single-Molecule Surface-Enhanced Raman Spectroscopy of Nonresonant Molecules. *J. Am. Chem. Soc.* **2009**, *131*, 14466–14472.

(49) Walker, S.; Oun, R.; McInnes, F. J.; Wheate, N. J. The Potential of Cucurbit[n]urils in Drug Delivery. *Isr. J. Chem.* **2011**, *51*, 616–624.

(50) García de Abajo, F.; Aizpurua, J. Numerical Simulation of Electron Energy Loss Near Inhomogeneous Dielectrics. *Phys. Rev. B* **1997**, *56*, 15873–15884.

(51) García de Abajo, F.; Howie, A. Retarded Field Calculation of Electron Energy Loss in Inhomogeneous Dielectrics. *Phys. Rev. B* **2002**, *65*, 115418.

(52) Johnson, P. B.; Christy, R. W. Optical Constants of the Noble Metals. *Phys. Rev. B* **1972**, *1318*, 4370–4379.